

# Model-based control strategies in the dynamic interaction of air supply and fuel cell

M Grujicic<sup>1\*</sup>, K M Chittajallu<sup>1</sup>, E H Law<sup>1</sup> and J T Pukrushpan<sup>2</sup>

<sup>1</sup>Department of Mechanical Engineering, Clemson University, Clemson, South Carolina, USA

<sup>2</sup>Automotive Research Center, Department of Mechanical Engineering, University of Michigan, Ann Arbor, Michigan, USA

**Abstract:** Model-based control strategies are utilized to analyse and optimize the transient behaviour of a polymer electrolyte membrane (PEM) fuel cell system consisting of air and fuel supply subsystems, a perfect air/fuel humidifier and a fuel cell stack at constant fuel cell temperature. The model is used to analyse the control of the fuel cell system with respect to maintaining a necessary level of oxygen partial pressure in the cathode during abrupt changes in the current demanded by the user. Maintaining the oxygen partial pressure in the cathode is necessary to prevent short circuit and membrane damage. The results obtained indicate that the oxygen level in the cathode can be successfully maintained through feedforward control of the air compressor motor voltage. However, the net power provided by the fuel cell system is compromised during the transients following abrupt changes in the stack current, suggesting a need for power management via the use of a secondary power source such as a battery.

**Keywords:** polymer electrolyte membrane, fuel cells

## NOTATION

$a$	water vapour activity
$c_v$	water concentration in the membrane (mol/m <sup>3</sup> )
$D_w$	diffusion coefficient of water in the membrane (m <sup>2</sup> /s)
$i$	local current density (A/m <sup>2</sup> )
$I$	current (A)
$K$	gain factor
$m$	mass (kg)
$n_d$	electroosmotic water drag coefficient in the membrane
$N$	rotational speed (r/min)
$p$	pressure (Pa)
PR	pressure ratio
$P$	power (kW)
$R$	resistance ( $\Omega$ )
$t$	time (s)
$T$	temperature (K)
$U$	speed (m/s)
$v$	voltage (V)
$V$	volume (m <sup>3</sup> )
$W$	flowrate (kg/s)

$\eta$	efficiency
$\mu$	water content
$\sigma$	conductivity ( $\Omega^{-1} \text{ m}^{-1}$ )
$\tau$	torque (N m)
$\phi$	relative humidity
$\omega$	rotational speed (rad/s)

## Subscripts

a	dry air related quantity
amb	quantity under ambient conditions
atm	quantity at 1 atm pressure
An	anode related quantity
cr	corrected quantity
crit	critical quantity
Ca	cathode related quantity
CM	compressor motor related quantity
Cp	compressor related quantity
d	downstream quantity
des	desired level of a quantity
fc	individual fuel cell related quantity
gen	quantity generated through electrochemical reaction
H <sub>2</sub>	hydrogen related quantity
in	inlet quantity
m	membrane related quantity
net	net quantity
N <sub>2</sub>	nitrogen related quantity
out	outlet quantity

The MS was received on 20 July 2003 and was accepted after revision for publication on 14 May 2004.

\*Corresponding author: 241 Engineering Innovation Building, Clemson, South Carolina 29634-0921, USA.

O <sub>2</sub>	oxygen related quantity
react	quantity consumed in electrochemical reaction
RM	quantity associated with the return manifold for the cathode
sat	level associated with water vapour saturation
st	fuel cell stack related quantity
SM	quantity associated with the supply manifold for the cathode
u	upstream quantity
v	water vapour related quantity
w	liquid water related quantity

### Superscripts

0	nominal value
opt	optimal value
max	maximum value

The remaining quantities are defined in Tables 1 and 2.

## 1 INTRODUCTION

Fuel cells are electrochemical devices that convert the chemical energy stored in gaseous fuel such as hydrogen directly into electricity. Fuel cells are typically classified according to the type of membrane (polymer electrolyte

**Table 1** General parameters used for modelling the PEM fuel cell system

Parameter	Symbol	SI units	Value
Atmospheric pressure	$p_{\text{atm}}$	Pa	$1.013 \times 10^5$
Atmospheric temperature	$T_{\text{atm}}$	K	298.15
Air specific heat ratio	$\gamma$	—	1.4
Air specific heat	$C_p$	J/kg K	1004
Air density	$\rho_a$	kg/m <sup>3</sup>	1.23
Universal gas constant	$R$	J/mol K	8.314
Air gas constant	$R_a$	J/kg K	286.9
Oxygen gas constant	$R_{O_2}$	J/kg K	259.8
Nitrogen gas constant	$R_{N_2}$	J/kg K	296.8
Vapour gas constant	$R_v$	J/kg K	461.5
Hydrogen gas constant	$R_{H_2}$	J/kg K	4124.3
Molar mass of air	$M_a$	kg/mol	$28.97 \times 10^{-3}$
Molar mass of oxygen	$M_{O_2}$	kg/mol	$32.0 \times 10^{-3}$
Molar mass of nitrogen	$M_{N_2}$	kg/mol	$28.0 \times 10^{-3}$
Molar mass of vapour	$M_v$	kg/mol	$18.02 \times 10^{-3}$
Molar mass of hydrogen	$M_{H_2}$	kg/mol	$2.0 \times 10^{-3}$
Faraday's constant	$F$	A s/mol	96 487
Temperature of fuel cell	$T_{\text{fc}}$	K	353

**Table 2** Input parameters used for modelling the PEM fuel cell system

Parameter	Symbol	SI units	Value
Motor constant	$k_t$	N m/A	0.0153
Motor constant	$R_{\text{CM}}$	ohm	0.82
Motor constant	$k_v$	V/(rad/s)	0.0153
Compressor efficiency	$\eta_{\text{Cp}}$	—	0.80
Compressor motor mechanical efficiency	$\eta_{\text{CM}}$	—	0.98
Number of cells in fuel cell stack	$n$	—	381
Fuel cell active area	$A_{\text{fc}}$	m <sup>2</sup>	$280 \times 10^{-4}$
Supply manifold volume	$V_{\text{SM}}$	m <sup>3</sup>	0.02
Single stack cathode volume	$V_{\text{Ca}}$	m <sup>3</sup>	0.01
Single stack anode volume	$V_{\text{An}}$	m <sup>3</sup>	0.005
Return manifold volume	$V_{\text{RM}}$	m <sup>3</sup>	0.005
Supply manifold outlet orifice constant	$k_{\text{SM,out}}$	kg/s/Pa	$0.3629 \times 10^{-5}$
Cathode outlet orifice constant	$k_{\text{Ca,out}}$	kg/s/Pa	$0.2177 \times 10^{-5}$
Membrane dry density	$\rho_{\text{m,dry}}$	kg/m <sup>3</sup>	$2 \times 10^3$
Membrane dry equivalent weight	$M_{\text{m,dry}}$	kg/mol	1.1
Membrane thickness	$t_m$	m	$1.275 \times 10^{-4}$
Compressor diameter	$d_{\text{Cp}}$	m	0.2286
Compressor and motor inertia	$J_{\text{Cp}}$	kg m <sup>2</sup>	$5 \times 10^{-5}$
Return manifold throttle discharge coefficient	$C_D$	—	0.0124
Return manifold throttle area	$A_T$	m <sup>2</sup>	0.002
Average ambient air relative humidity	$\phi_{\text{atm}}$	—	0.5
Oxygen mole fraction at cathode inlet	$x_{O_2,\text{in}}$	—	0.21
Hydrogen mole fraction at anode inlet	$x_{H_2,\text{in}}$	—	1.0

membrane fuel cells, solid oxide fuel cells, molten carbonate fuel cells, etc.) that they use to separate the anode and the cathode. Owing to their high energy efficiency, low-temperature ( $\sim 333$ – $353$  K) operation, pollution-free character and relatively simple design, so-called polymer electrolyte membrane (PEM) fuel cells are currently being considered as an alternative source of power in electric vehicles. However, in order to be able to compete successfully with internal combustion (IC) engines, PEM fuel cells (PEMFCs) must operate and function at least as well as IC engines. Specifically, the transient behaviour of PEMFCs following abrupt changes in the power demanded by the vehicle is particularly critical since it entails the control of the air and fuel flow, pressure regulation and heat and water management to maintain optimal temperature, membrane hydration and partial pressure of the reactants across the membrane and thus prevents fuel cell stack voltage degradation, maintains high efficiency and extends the fuel cell life [1].

The development of PEMFCs and the testing of their transient behaviour is quite costly and time consuming, and thus the use of mathematical modelling has become an important tool in fuel cell development. Over the last decade, a number of fuel cell models have been developed. Most of these models, including the ones developed by Grujicic and Chittajallu [2–4], are steady state, single-cell models that include spatial variation in the fuel cell parameters and are based on electrochemical, thermodynamic and fluid mechanical principles. While these models have made a major contribution to understanding the effect of various operating, geometrical and material parameters on the fuel cell performance and have been successfully used in the optimization of fuel cell design, they are not suitable for analysis and control of the transient behaviour of fuel cells.

Only a few dynamic fuel cell models have been proposed so far, and most of them address issues specific to the control of particular fuel cell subsystems (e.g. references [5] and [6]). Recently, Pukrushpan *et al.* [7, 8] proposed a fuel cell system dynamic model suitable for control of fuel cell transient behaviour. The model deals with the fuel cell stack system and includes the flow and inertia characteristics of the air compressor and the cathode and anode manifold filling dynamics. In the present work, the model of Pukrushpan *et al.* [7, 8] has been extended to include the effect of optimization of the oxygen ratio in the cathode which yields a maximum net power at a given level of fuel cell stack current.

The organization of the paper is as follows. The model of Pukrushpan *et al.* [7, 8] is briefly outlined in section 2. The computational procedure used is discussed in section 3. The main results obtained in the present work are presented and discussed in section 4. The main conclusions resulting from the present work are summarized in section 5.

## 2 MODEL

Control-oriented models of fuel cell systems have a number of salient features:

1. They include dynamic (transient) effects, while the effects of spatial variation in the model parameters are neglected.
2. Since the dynamics of electrochemical reactions and of the electrode electrical response is associated with very fast transients, their effects on the overall fuel cell system transient performance is minimal and is neglected.
3. Transient behaviour of manifold filling, of membrane hydration, of the air compressor and of the heat management is significantly more sluggish and, hence, should be included in the model.

4. Interactions between the processes identified in (3) should also be taken into account.
5. Owing to its relatively slow transient response, the dynamics of the fuel cell stack temperature may play an important role. However, the stack temperature is generally considered to be controlled separately from the rest of the fuel cell system and its average value to be well regulated.
6. The humidity and the temperature of the inlet reactant flows in the cathode and the anode are generally assumed to be controlled in a fast manner so that the effect of their transient behaviours is not typically considered.

In this section, a brief outline is given of the fuel cell stack dynamic model proposed by Pukrushpan *et al.* [7, 8]. A schematic of the PEMFC system analysed in the model is shown in Fig. 1.

### 2.1 State-space representation

The model proposed by Pukrushpan *et al.* [7, 8] uses the following nine states: the mass of oxygen in the cathode,  $m_{O_2}$  (kg), the mass of nitrogen in the cathode,  $m_{N_2}$  (kg), the mass of water in the cathode,  $m_{w,Ca}$  (kg), the mass of hydrogen in the anode,  $m_{H_2}$  (kg), the mass of water in the anode,  $m_{w,An}$  (kg), the compressor speed,  $\omega_{Cp}$  (rad/s), the supply manifold pressure,  $p_{SM}$  (Pa), the mass of air in the supply manifold,  $m_{SM}$  (kg), and the return manifold pressure,  $p_{RM}$  (Pa).

### 2.2 Governing equations

The governing equations for the mass of air in the supply manifold, for the masses of oxygen, nitrogen and water in the cathode and for the masses of hydrogen and water in

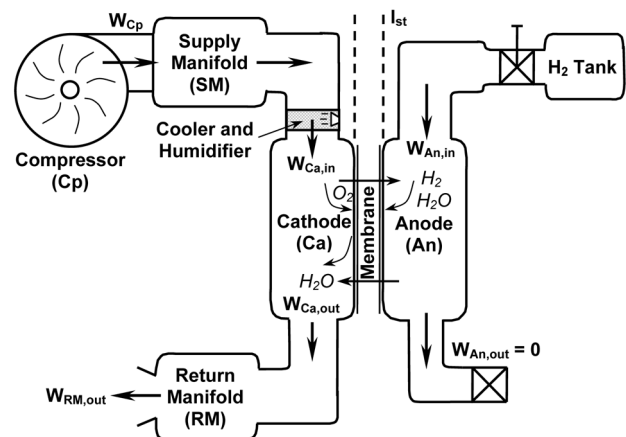


**Fig. 1** Schematic of the PEM fuel cell system analysed in the present work

the anode are respectively defined using the principle of mass conservation as

$$\frac{dm_{SM}}{dt} = W_{Cp} - W_{SM,out} \quad (1)$$

$$\frac{dm_{O_2}}{dt} = W_{O_2,in} - W_{O_2,out} - W_{O_2,react} \quad (2)$$

$$\frac{dm_{N_2}}{dt} = W_{N_2,in} - W_{N_2,out} \quad (3)$$

$$\frac{dm_{w,Ca}}{dt} = W_{v,Ca,in} - W_{v,Ca,out} + W_{v,Ca,gen} + W_{v,m} \quad (4)$$

$$\frac{dm_{H_2}}{dt} = W_{H_2,in} - W_{H_2,out} - W_{H_2,react} \quad (5)$$

$$\frac{dm_{w,An}}{dt} = W_{v,An,in} - W_{v,An,out} - W_{v,m} \quad (6)$$

Besides the standard input and output fluxes, equations (2) to (6) also contain reaction-generated flux terms (subscript 'gen'), reaction-based sink terms (subscript 'react') and a term associated with the transport of water through the membrane (subscript 'm'). It should be noted that, since, under standard operating conditions, water condensation due to vapour saturation can occur, a distinction is made between vapour and water (where the latter includes both the liquid and gaseous states of H<sub>2</sub>O).

The governing equation for the rotational speed of the compressor is defined by the power conservation principle as

$$J_{Cp} \frac{d\omega_{Cp}}{dt} = \tau_{CM} - \tau_{Cp} \quad (7)$$

The governing equations for the supply manifold pressure and for the return manifold pressure are respectively defined using the energy conservation principle and standard thermodynamic relationships as

$$\frac{dp_{SM}}{dt} = \frac{\gamma R_a}{V_{SM}} (W_{Cp} T_{Cp} - W_{SM,out} T_{SM}) \quad (8)$$

$$\frac{dp_{RM}}{dt} = \frac{R_a T_{RM}}{V_{RM}} (W_{Ca,out} - W_{RM,out}) \quad (9)$$

### 2.3 Closure relations

To express the governing equations in terms of the states, the following closure relations are used. The compressor air flowrate,  $W_{Cp}$ , is related to the supply manifold pressure,  $p_{SM}$ , and the compressor motor rotational speed,  $\omega_{Cp}$ , via the appropriate static compressor map [9] as reviewed in Appendix 1. The supply manifold outlet air rate,  $W_{SM,out}$ , is related to  $p_{SM}$  and  $p_{Ca}$  via the linearized nozzle equation

$$W_{SM,out} = k_{SM,out} (p_{SM} - p_{Ca}) \quad (10)$$

The inlet oxygen, nitrogen and cathode vapour mass flowrates,  $W_{O_2,in}$ ,  $W_{N_2,in}$  and  $W_{v,Ca,in}$  are related to the cathode inlet air mass flowrate, the inlet air humidity and the mass

fraction of oxygen and nitrogen in dry air using the ideal gas relations. The outlet oxygen, nitrogen and cathode vapour mass flowrates,  $W_{O_2,out}$ ,  $W_{N_2,out}$  and  $W_{v,Ca,out}$ , are likewise related to the outlet air mass flowrate, the outlet air humidity and the mass fraction of the oxygen and nitrogen in dry air at the cathode outlet using the ideal gas relations.

The reacted oxygen and hydrogen and generated water vapour (in the cathode) mass flowrates,  $W_{O_2,react}$ ,  $W_{H_2,react}$  and  $W_{v,Ca,gen}$ , are related to the fuel cell stack current

$$W_{O_2,react} = M_{O_2} \frac{nI_{st}}{4F} \quad (11)$$

$$W_{H_2,react} = M_{H_2} \frac{nI_{st}}{2F} \quad (12)$$

$$W_{v,Ca,gen} = M_v \frac{nI_{st}}{2F} \quad (13)$$

where 4 and 2 in the denominators denote the number of electrons involved in the oxidation and the reduction half-reactions respectively.

The water mass flowrate through the membrane,  $W_{v,m}$ , is defined using the membrane hydration model given in Appendix 2. The outlet hydrogen and water masses in the anode are assumed to be zero, that is, hydrogen is assumed to react completely in the anode, while water generated by the oxidation half-reaction is assumed to be transported via electroosmosis through the membrane towards the cathode.

The compressor motor torque,  $\tau_{CM}$ , is related to the compressor motor voltage,  $v_{CM}$ , and the compressor motor rotational speed by the static motor equation

$$\tau_{CM} = \eta_{CM} \frac{k_t}{R_{CM}} (v_{CM} - k_v \omega_{Cp}) \quad (14)$$

The steady state compressor torque,  $\tau_{Cp}$ , is related to the supply manifold pressure, the compressor motor rotational speed and the compressor air flowrate via the thermodynamic relations

$$\tau_{Cp} = \frac{C_p}{\omega_{Cp}} \frac{T_{atm}}{\eta_{Cp}} \left[ \left( \frac{p_{SM}}{p_{atm}} \right)^{(\gamma-1)/\gamma} - 1 \right] W_{Cp} \quad (15)$$

The air temperature in the compressor,  $T_{Cp}$ , is defined using basic thermodynamic relations

$$T_{Cp} = T_{atm} + \frac{T_{atm}}{\eta_{Cp}} \left[ \left( \frac{p_{SM}}{p_{atm}} \right)^{(\gamma-1)/\gamma} - 1 \right] \quad (16)$$

The air temperature in the supply manifold,  $T_{SM}$ , is obtained from  $m_{SM}$ ,  $p_{SM}$  and  $V_{SM}$  using the ideal gas law.

The cathode outlet air flowrate,  $W_{Ca,out}$ , is related to the cathode pressure and return manifold pressure via a linearized nozzle equation analogous to that in equation (10). The return manifold outlet air flowrate,  $W_{RM,out}$ , is defined using a non-linearized nozzle relation as discussed in Appendix 3,

while the return manifold air temperature,  $T_{RM}$ , is considered to be constant and equal to the temperature of the fuel cell stack.

### 3 COMPUTATIONAL METHOD

Nine first-order non-linear ordinary differential equations [equations (1) to (9)] are solved using the commercial mathematical and visualization package MATLAB [10]. The ODE23s MATLAB solver based on a combination of second- and third-order Runge–Kutta methods is used. This solver is suitable for solving stiff differential equations whose response changes rapidly over a time-scale that is short compared with the time-scale over which the solution is sought.

The design of a non-linear feedforward controller, discussed in section 4.2, is carried out using the control system toolbox of the MATLAB program [10]. The control system toolbox is a collection of algorithms that implement common control system design, analysis and modelling techniques.

## 4 RESULTS AND DISCUSSION

### 4.1 Maximization of the net power

The net power of a fuel cell system,  $P_{net}$ , can be approximately defined as the difference between the power produced by the stack,  $P_{st}$ , and the power required to run the air compressor motor,  $P_{CM}$ . At a given stack current,  $I_{st}$ , an increase in the compressor flowrate increases the cathode pressure (and thus the oxygen partial pressure) and, in turn, the stack voltage. This also leads to a higher level of the excess amount of oxygen in the cathode which is generally defined as the ratio between the rate at which oxygen is supplied and the rate at which oxygen is consumed in the cathode, i.e.  $\lambda_{O_2} = W_{O_2,in}/W_{O_2,react}$ . As  $\lambda_{O_2}$  is initially increased by increasing the compressor motor voltage, both  $P_{st}$  and  $P_{net}$  are increased. However, a further increase in  $\lambda_{O_2}$  generally requires an excessive increase in the compressor motor voltage which causes  $P_{net}$  to begin to decrease. Thus, at each level of the stack current there is an optimal value of  $\lambda_{O_2}$  at which  $P_{net}$  takes on the maximum value. This can be seen in Fig. 2 in which the variation in  $P_{net}$  with  $\lambda_{O_2}$  is displayed for different levels of stack current. The results displayed in Fig. 2 pertain to typical fuel cell operating conditions ( $T_{fc} = 353$  K,  $\phi_{Ca} = 1$ ) and are obtained by solving equations (1) to (9) under the steady state condition.

The corresponding variation in maximum net power,  $P_{net}^{max}$ , optimal oxygen ratio,  $\lambda_{O_2}^{opt}$ , optimal supply manifold air pressure,  $p_{SM}^{opt}$ , and optimal compressor motor voltage,  $v_{CM}^{opt}$ , with stack current is shown in Figs 3a to d. While the observed increases in  $P_{net}^{max}$ ,  $p_{SM}^{opt}$  and  $v_{CM}^{opt}$  with stack current are anticipated, the variation in  $\lambda_{O_2}^{opt}$  with  $I_{st}$  indicates that, at higher stack currents, maintaining high  $\lambda_{O_2}$  values entails high power consumption by the compressor motor so that  $\lambda_{O_2}^{opt}$  decreases as  $I_{st}$  increases.

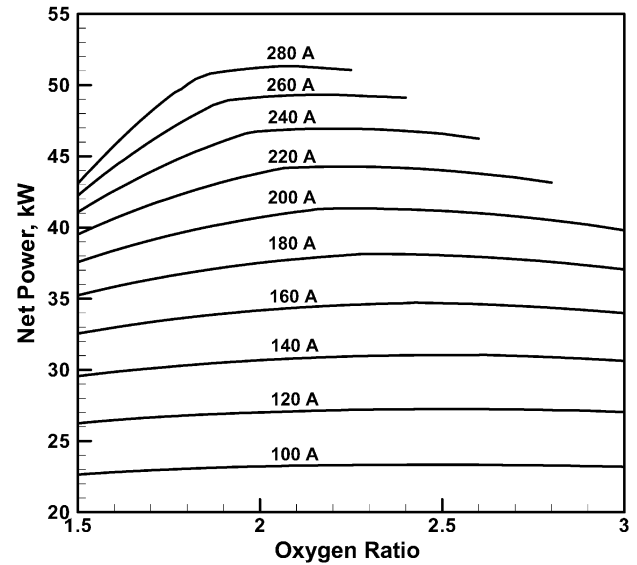


Fig. 2 Variation in net power with oxygen ratio at different stack current levels under standard operating conditions:  $T_{fc} = 353$  K and  $\phi_{Ca} = 1$

### 4.2 Control problem formulation

In a fuel cell system there are three main control systems which regulate:

- the air/fuel supply,
- the water supply,
- the heat management.

In the present model, a perfect air/fuel humidifier and a perfect air and stack cooler are postulated. In addition, a fast proportional feedback fuel flow controller, which ensures a zero pressure difference across the membrane, is assumed. Therefore, the control problem discussed in the present work focuses on the regulation of the air (i.e. oxygen) supply to the cathode.

As shown in the previous section, at each level of stack current, there is an optimal value of the compressor motor voltage,  $v_{CM}^{opt}$ , which maximizes the stack net power,  $P_{net}^{max}$ . As seen in Fig. 3d, the variation in the optimal  $v_{CM}^{opt}$  with  $I_{st}$  can be quite successfully expressed using a second-order polynomial. When the current demand from the vehicle suddenly increases, the oxygen consumption in the cathode also increases and, hence, the oxygen partial pressure drops. The accompanying drop in the fuel cell voltage may lead to a short circuit and/or membrane damage, the phenomenon known as *oxygen starvation*. To prevent this from happening, the air supply must be increased as quickly as possible to replenish the cathode with oxygen. Also, the fuel supply to the anode must be quickly adjusted to ensure a minimum pressure difference across the fuel cell membrane. A similar control of the fuel cell system is required during a sudden drop in the stack current.

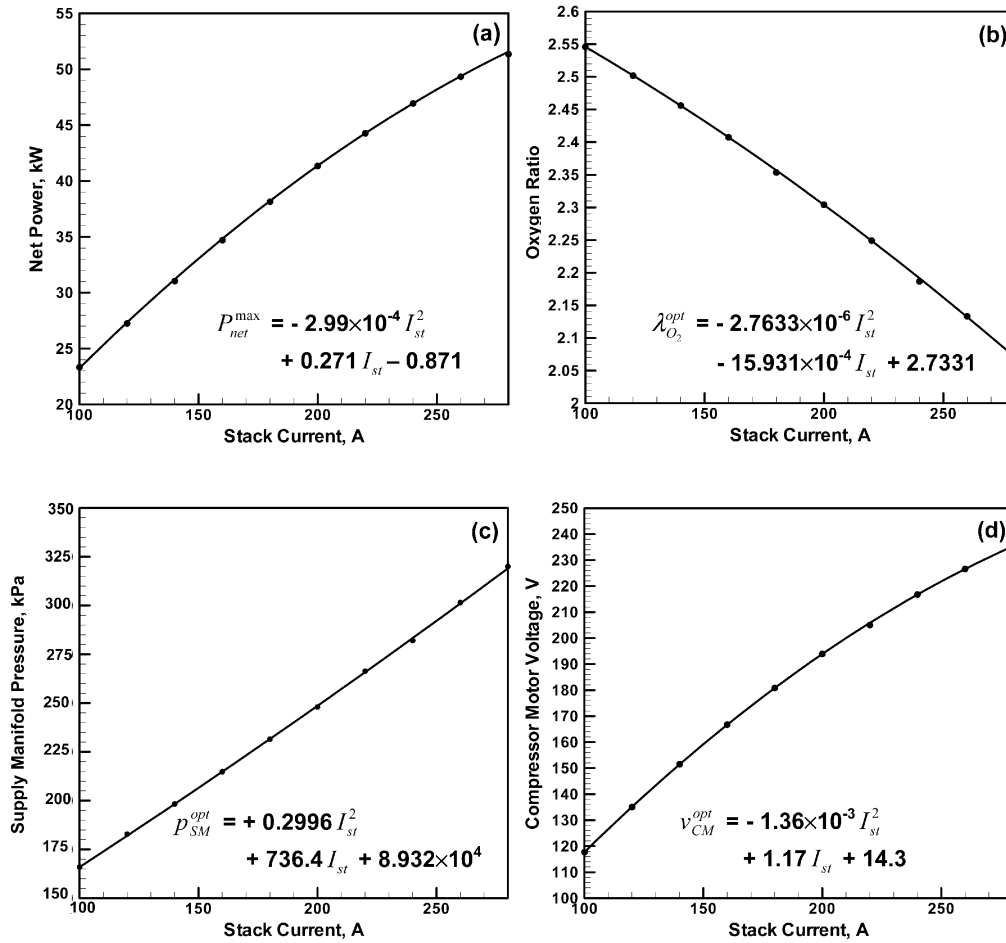


**Fig. 3** (a) Maximum net power, (b) optimal oxygen ratio, (c) optimal supply manifold pressure and (d) optimal compressor motor voltage as functions of stack current in a PEM fuel cell under standard operating conditions

Thus, the fuel cell system control problem can be defined as

State equations

$$\dot{\mathbf{x}} = f(\mathbf{x}, \mathbf{u}, \mathbf{w}) \quad (17)$$

States

$$\mathbf{x} = [m_{O_2} \ m_{H_2} \ m_{N_2} \ \omega_{Cp} \ p_{SM} \ m_{SM} \ m_{w,An} \ m_{w,Ca} \ p_{RM}]^T$$

Controlled variable

$$\mathbf{u} = v_{CM}$$

Disturbance

$$\mathbf{w} = I_{st}$$

Performance Variables

$$\mathbf{z} = [z_1 = P_{net} - P_{net}^{max}, z_2 = \lambda_{O_2} - \lambda_{O_2}^{opt}]^T = h_z(\mathbf{x}, \mathbf{u}, \mathbf{w})$$

Measurements

$$\mathbf{y} = [p_{SM}, p_{An}]^T$$

It should be noted that the two control objectives,  $z_1 = z_2 = 0$ , are achievable at steady state, but their transients differ considerably and hence cannot be regulated simultaneously using a single control variable,  $v_{CM}$ . Owing to the above-mentioned consequences of oxygen starvation, the control of the transient behaviour of  $\lambda_{O_2}$  is deemed more critical in this work. The control of the transient behaviour of the net power is not considered and is assumed to be achieved through power management via a secondary power source (a battery). Furthermore, as mentioned above, the goal of the hydrogen flow control is to minimize the pressure difference across the membrane. Hydrogen is supplied to the anode from a high-pressure tank, and its flowrate is controlled by a valve. Since the valve has a fast response, the hydrogen flowrate can be directly regulated using a proportional feedback controller based on the anode/cathode pressure difference. In practice, however,

the cathode and anode pressures cannot be directly measured. To overcome this problem on the cathode side, the supply manifold pressure and a nominal supply manifold/cathode pressure drop are used in place of the cathode pressure. The anode supply manifold, on the other hand, is typically small and its volume is lumped in the present model with the anode volume. The anode pressure can then be considered as being practically equal to the measured pressure in the anode supply manifold. Hence, the fuel inlet flowrate can be defined as  $W_{An,in} = K_1(K_2 p_{SM} - p_{An})$ , where  $K_1$  is the proportional gain and  $K_2 = p_{Ca}/p_{SM}$  is the pressure drop between the cathode supply manifold and the cathode. The fuel supply feedback controller hence entails the measurement of two variables,  $p_{SM}$  and  $p_{An}$ . As far as the control of  $\lambda_{O_2}$  is concerned, only the open-loop (static and dynamic) feedforward strategies (as shown schematically in Figs 4a to b) will be considered in this paper.

#### 4.2.1 Open-loop/static feedforward controller

Since the stack current,  $I_{st}$ , which acts as a disturbance to  $\lambda_{O_2}$ , can be readily measured, and since the relationship between  $v_{CM}^{opt}$  and  $I_{st}$  is known (Fig. 3d), the value of  $v_{CM}^{opt}$  that maximizes the net power at a given level of stack current can be computed and used in the static feedforward control. The results of implementation of the static feedforward controller are displayed in Figs 5a to d.

The time evolution of the stack current (consisting of a number of steps) which acts as an input disturbance to the system is shown in Fig. 5a. The corresponding optimal values of the compressor motor voltage  $v_{CM}^{opt}$  (the control variable) are displayed (using dashed lines) in Fig. 5b.

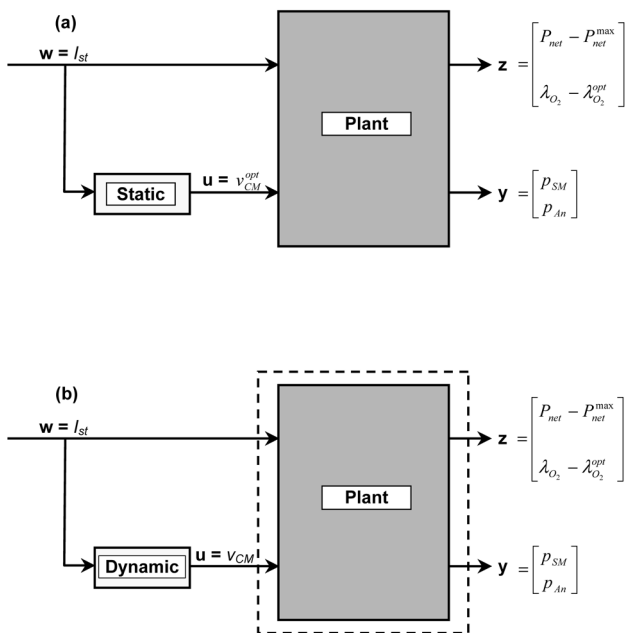


**Fig. 4** (a) Static and (b) dynamic open-loop feedforward control of the PEM fuel cell system

The corresponding optimal level of the oxygen ratio is shown as dotted lines in Fig. 5c. The temporal evolution of the oxygen ratio associated with implementation of the static feedforward controller is also displayed in Fig. 5c but using dashed lines. The corresponding maximum value and (static feedforward controlled) temporal evolution of the net power are shown as dotted and dashed lines in Fig. 5d, respectively. To enhance the clarity, selected portions of Figs 5b to d have been magnified and displayed as insets.

The dynamic transition between different compressor flowrates and pressure conditions associated with the temporal evolution of the system disturbance (Fig. 5a) in the fuel cell system regulated via the static feedforward controller is displayed (as solid lines) on the compressor map in Fig. 6a. The corresponding voltage/current density response of the fuel cell is shown also as solid lines in Fig. 6b. Arrows and numbers (time in seconds) are used in Figs 6a and b to indicate respectively the supply manifold/atmospheric pressure ratio/flowrate and cell voltage/current density trajectories. The results displayed in Fig. 6a can be used to identify stack current changes that may produce a surge or a stall of the compressor. For example, there is an indication of compressor stall at times between 5–7 and 10–12 s. It should also be noted that times 0 and 25 s in Fig. 6b are used to indicate the beginning and the end of simulations.

#### 4.2.2 Open-loop/dynamic feedforward controller

In this section, a dynamic feedforward controller is designed that more effectively cancels the disturbance of  $\lambda_{O_2}$  caused by  $I_{st}$  during the transient. To develop such a controller, the plant (surrounded by a dashed-line box in Fig. 4b) is first linearized around a nominal operating point associated with the maximum net power  $P_{net}^{max} = 39.825$  kW, the optimal oxygen ratio  $\lambda_{O_2}^{opt} = 2.33$ , the stack current  $w^0 = I_{st} = 190$  A and the compressor motor voltage  $u^0 = v_{CM}^{opt} = 187.5$  V, where a superscript zero is used to denote the nominal value of a quantity. Linearization of the non-linear model defined by equations (1) to (9) is done by imposing a small perturbation around the nominal point to one of the states, the disturbance or the control variable at a time and quantifying the system response using a finite difference method. The resulting linearized model can be expressed as

$$\begin{aligned} \delta \dot{x} &= \mathbf{A} \delta x + \mathbf{B}_u \delta u + \mathbf{B}_w \delta w \\ \delta z &= \mathbf{C}_z \delta x + \mathbf{D}_{zu} \delta u + \mathbf{D}_{zw} \delta w \end{aligned} \quad (18)$$

where  $\delta$  is used to denote the variation in a quantity from its nominal value.

The linearized system matrices  $\mathbf{A}$ ,  $\mathbf{B}_u$ ,  $\mathbf{B}_w$ ,  $\mathbf{C}_z$ ,  $\mathbf{D}_{zu}$  and  $\mathbf{D}_{zw}$  are listed in Appendix 5. The analysis carried out in section 4.1 revealed that  $m_{w,Ca}$  is associated with fully humidified air, and hence this state is not observable and is not considered in the design of the dynamic feedforward

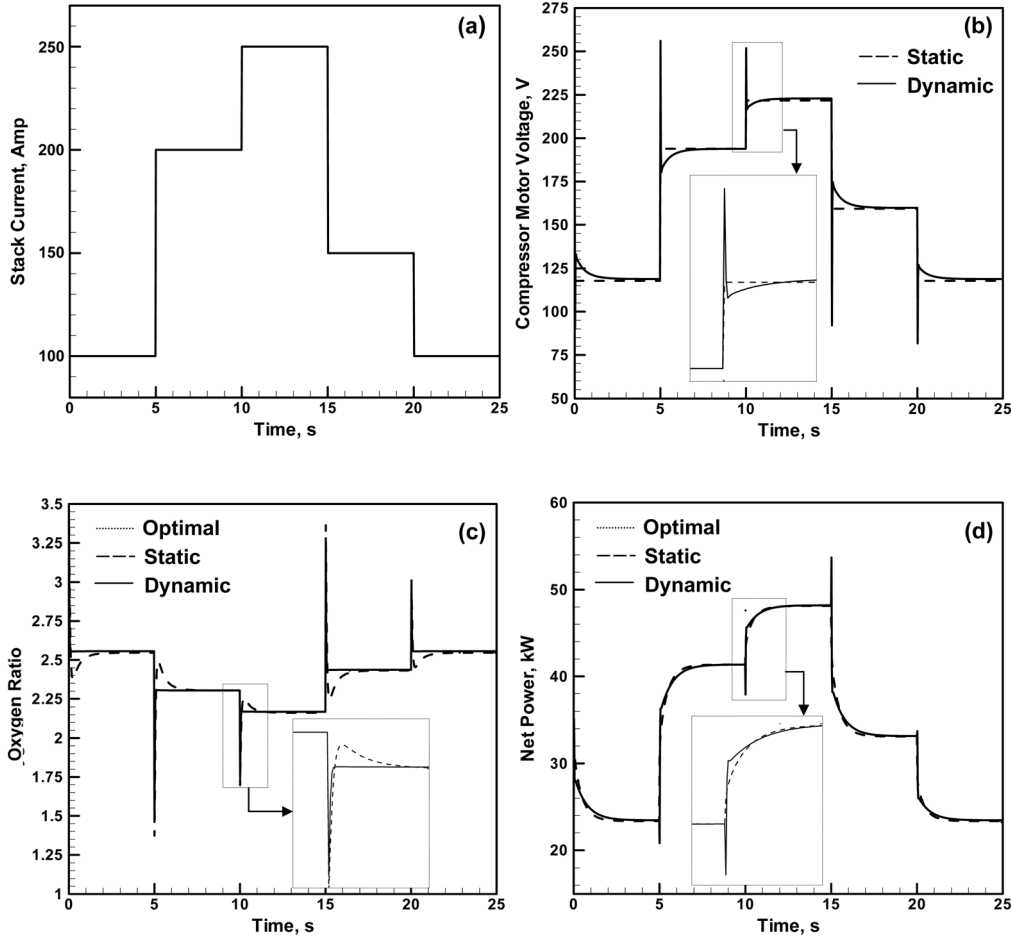


**Fig. 5** (a) Step-like temporal variation in the (input) stack current, and the corresponding (b) compressor motor voltage, (c) oxygen ratio and (d) net power optimal and statically and dynamically feedforward controlled levels

controller. In other words, the linearized system has eight states, one less than the original system.

Application of the Laplace transform to equation (18) yields

$$\Delta Z_2 = G_{z_2u} \Delta U + G_{z_2w} \Delta W \quad (19)$$

where  $G_{z_2u} = \mathbf{C}_{z_2}(s\mathbf{I} - \mathbf{A})^{-1}\mathbf{B}_u + \mathbf{D}_{z_2u}$ ,  $G_{z_2w} = \mathbf{C}_{z_2}(s\mathbf{I} - \mathbf{A})^{-1}\mathbf{B}_w + \mathbf{D}_{z_2w}$ ,  $s$  is the Laplace variable and all the quantities denoted using capital letters are expressed in the Laplace domain.

The dynamic feedback controller is then defined as

$$\Delta U = K_{uw} \Delta W \quad (20)$$

The ideal controller,  $K_{uw}^{\text{ideal}}$ , of the compressor motor voltage is constructed in such a way that the transfer function from disturbance  $\Delta W$  to performance  $\Delta Z_2$

$$T_{z_2w} = \frac{\Delta Z_2(s)}{\Delta W(s)} = (G_{z_2w} + G_{z_2u}K_{uw}) \quad (21)$$

is equal to zero. This ensures a complete disturbance rejection and yields

$$K_{uw}^{\text{ideal}} = -G_{z_2u}^{-1}G_{z_2w} \quad (22)$$

Since  $G_{z_2u}$  is minimum phase (all its zeros have a negative real part) and  $G_{z_2w}$  is stable (all its poles have a negative real part),  $K_{uw}^{\text{ideal}}$  is a stable controller. However,  $K_{uw}^{\text{ideal}}$  is not proper (the order of the polynomial in the numerator is higher than that of the denominator). In addition, through the use of the standard frequency response analysis, it is found that  $K_{uw}^{\text{ideal}}$  leads to a progressively higher magnitude of the control input at high frequencies. To overcome these problems, a low-pass filter is applied to  $K_{uw}^{\text{ideal}}$  to obtain

$$K_{uw} = -\frac{1}{(1 + s/\alpha_1)(1 + s/\alpha_2)(1 + s/\alpha_3)} G_{z_2u}^{-1}G_{z_2w} \quad (23)$$

Using the standard frequency analysis, it is further found that setting  $\alpha_1$ ,  $\alpha_2$  and  $\alpha_3$  to 80, 120 and 120 respectively prevents excessive rise in the magnitude of  $K_{uw}$  at high

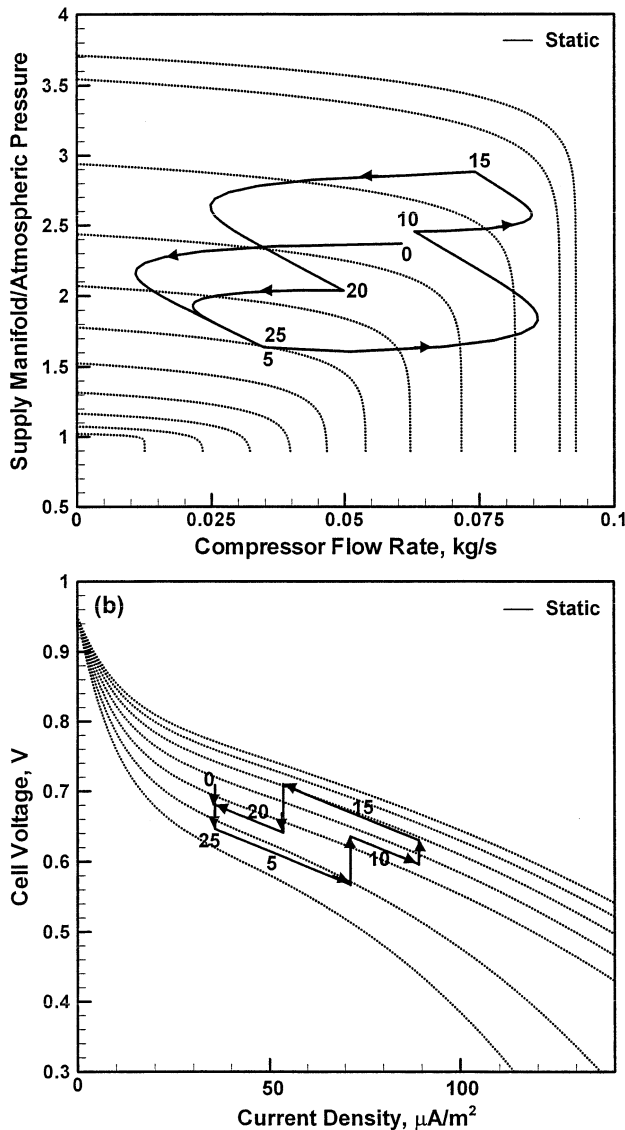


**Fig. 6** Temporal responses of (a) the compressor and (b) the fuel cell corresponding to the changes in the stack current displayed in Fig. 5a under static feedforward control of the compressor motor voltage. The numbers refer to the time in seconds

frequencies. Larger values of  $\alpha_1$ ,  $\alpha_2$  and  $\alpha_3$  can be used to speed up the response of the system, but at the expense of larger compressor motor power expended.

The dynamic feedforward controller obtained is as follows

$$K_{uw} = \frac{5.5193 \times 10^2 s^6 + 8.7183 \times 10^4 s^5 + 4.0733 \times 10^6 s^4 + 6.2444 \times 10^7 s^3 + 2.7798 \times 10^8 \times s^2 + 4.6365 \times 10^8 s + 2.6044 \times 10^8}{s^7 + 3.9246 \times 10^2 s^6 + 5.7151 \times 10^4 s^5 + 3.7038 \times 10^6 s^4 + 9.5901 \times 10^7 s^3 + 4.3987 \times 10^8 \times s^2 + 7.0891 \times 10^8 s + 3.7923 \times 10^8} \quad (24)$$

Inversion of  $K_{uw}$  from the Laplace domain into the time domain is then used to obtain the time trajectory of the compressor motor voltage needed to reject the disturbance associated with the stack current profile given in Fig. 5a.

The results of implementation of the dynamic feedforward controller to regulate  $\lambda_{O_2}$  subject to  $I_{st}$  disturbance shown in Fig. 5a are displayed (as solid lines) in Figs 5b to d. The corresponding compressor flow/pressure and fuel cell voltage/current density results for the fuel cell system regulated by the dynamic feedforward controller are quite similar to their counterparts for the static feedforward control, and hence are not displayed in Figs 6a and b respectively.

A comparison of the fuel cell system performance results (the oxygen ratio and the net power) displayed in Figs 5c and d for the statically and dynamically feedforward controlled original system shows that the use of the dynamic controller reduces the rise and the settling times for  $\lambda_{O_2}$  but at the expense of larger excursions in the net power during the transient. Furthermore, a comparison of the corresponding results displayed in Figs 5b and d shows that, in the case of the dynamic feedforward control, the transient behaviour of the net power correlates with the transient behaviour of the control variable, the compressor motor voltage. Since the transient behaviour of the compressor motor voltage was designed with the objective of rejecting  $\lambda_{O_2}$  disturbances, and the compressor motor voltage is the only control variable, the net power performance is compromised. Hence, a separate power management system is needed to avoid large excursions in the fuel cell system net power following abrupt changes in the stack current.

It should be noted that, in spite of the fact that the dynamic feedforward controller reduces the  $\lambda_{O_2}$  disturbances over a wide range of frequencies, as other feedforward controllers, it suffers from a lack of ability to handle unknown disturbances, modelling errors and potential variations in the model parameters. In addition, a careful observation of the insets in Figs 5b to d reveals the presence of linearization-induced steady state errors. Moreover, sensitivity of the system to unknown disturbances is unity at all frequencies, making the system not very robust. While the controller sensitivity can be reduced (provided the range of plant uncertainty is known) through frequency domain modification, all the deficiencies of the feedforward controller discussed above will be addressed in a companion paper using the feedback control approach.

## 5 CONCLUSIONS

Based on the results obtained in this paper, the following main conclusions can be drawn:

1. While the model presented in this paper is not fully validated, it is found to capture the basic transient behaviour of a PEM fuel cell system including flow characteristics

- and dynamics of the air compressor motor and the supply manifold filling.
2. A static or a dynamic feedforward control scheme can be readily implemented to prevent large excursions in the oxygen ratio during abrupt changes in the stack current. However, sensitivity of such schemes to external disturbances, errors in model parameters as a result of equipment ageing and the presence of steady state errors indicates a need for the use of a feedback controlling scheme.
  3. Maintaining the necessary level of oxygen to prevent the occurrence of the oxygen starvation phenomenon, achieved through the use of a feedforward control, is done at the expense of the net power transient behaviour, indicating the need for a separate power management strategy.
  4. It could be noted that, although these first results lead to only relatively small improvements, future use of control theory for fuel cell systems may be very fruitful; for example, when coupling a battery and power management, as indicated in this paper, is applied.

## ACKNOWLEDGEMENTS

The authors are indebted to Drs Imtiaz Haque, Frank Paul and John Wagner for stimulating discussions. The authors also acknowledge the support of the Office of High-Performance Computing Facilities at Clemson University.

## REFERENCES

- 1 Yang, W.-C., Bates, B., Fletcher, N. and Pow, R. Control challenges and methodologies in fuel cell vehicle development. SAE paper 98C054, 1998.
- 2 Grujicic, M. and Chittajallu, K. M. Design and optimization of polymer electrolyte membrane (PEM) fuel cells. *Appl. Surf. Sci.*, 2004, **227**, 56.
- 3 Grujicic, M. and Chittajallu, K. M. Geometrical optimization of the cathode in polymer electrolyte membrane (PEM) fuel cells. *Chem. Engng Sci.*, submitted for publication, December 2003.
- 4 Grujicic, M., Zhao, C. L., Chittajallu, K. M. and Ochterbeck, J. M. Cathode and interdigitated air distributor optimizations in polymer electrolyte membrane (PEM) fuel cells. *Mater. Sci. and Engng*, 2004, **B30**, 30.
- 5 Hauer, K. H., Friedmann, D. J., Moore, R. M., Ramaswamy, S., Eggert, A. and Badrinarayana, P. Dynamic response of an indirect-methanol fuel cell vehicle. SAE paper 2000-01-370, 2000.
- 6 Pischinger, S., Schonfelder, C., Borscheuer, W., Kindl, H. and Wiartalla, A. Integrated air supply and humidification concepts for fuel cell systems. SAE paper 2001-01-0233, 2001.
- 7 Pukrushpan, J. T., Peng, H. and Stefanopoulou, A. G. Simulation and analysis of transient fuel cell system performance based on a dynamic reactant flow model. ASME International Mechanical Engineering Congress and Exposition, New Orleans, Louisiana, 17–22 November 2002.

- 8 Pukrushpan, J. T., Stefanopoulou, A. G. and Peng, H. Modeling and control for PEM fuel cell stack system. Proceedings of American Control Conference, Anchorage, Alaska, 2002, pp. 3117–3122.
- 9 Cunningham, J. M., Hoggman, M. A., Moore, R. M. and Friedman, D. J. Requirements for a flexible and realistic air supply model for incorporation into a fuel cell vehicle (FCV) system simulation. SAE paper 1999-01-2912, 1999.
- 10 MATLAB, *The Language of Technical Computing*, 6th edition, 2000 (The MathWorks Incorporated, Natick, Massachusetts).
- 11 Moraal, P. and Kolmanovsky, I. Turbocharger modeling for automotive control applications. SAE paper 1999-01-0908, 1999.
- 12 Pukrushpan, J. T. Modeling and control of fuel cell systems and fuel processors. PhD thesis, University of Michigan, Ann Arbor, Michigan, 2003.
- 13 Thomas, P. *Simulation of Industrial Processes for Control Engineer*, 1999 (Butterworth-Heinemann, London).

## APPENDIX 1

### Compressor flowrate

The mass flowrate of the air in the compressor is determined using the method proposed by Jensen and Kristensen [11] for non-linear curvefitting of the compressor map

$$W_{Cp} = W_{cr} \frac{\delta}{\sqrt{\theta}} \quad (25)$$

where the corrected flowrate is given as

$$W_{cr} = \Phi \rho_a \frac{\pi}{4} d_{Cp}^2 U_{Cp} \quad (26)$$

while the normalized compressor flowrate is given as

$$\Phi = \Phi_{\max} \left\{ 1 - \exp \left[ \beta \left( \frac{\Psi}{\Psi_{\max}} - 1 \right) \right] \right\} \quad (27)$$

with  $\Phi_{\max}$ ,  $\beta$  and  $\Psi_{\max}$  being polynomial functions of the Mach number,  $M$

$$\Phi_{\max} = a_4 M^4 + a_3 M^3 + a_2 M^2 + a_1 M + a_0 \quad (28)$$

$$\beta = b_2 M^2 + b_1 M + b_0 \quad (29)$$

$$\Psi_{\max} = c_5 M^5 + c_4 M^4 + c_3 M^3 + c_2 M^2 + c_1 M + c_0 \quad (30)$$

The dimensionless head parameter is defined as

$$\Psi = \frac{C_p T_{Cp,in} [(p_{Cp,out}/p_{Cp,in})^{(\gamma-1)/\gamma} - 1]}{\frac{1}{2} U_{Cp}^2} \quad (31)$$

**Table 3** Regression coefficients in equations (28) to (30)

	Regression coefficient		
	$a_i$	$b_i$	$c_i$
$i = 0$	$2.21195 \times 10^{-3}$	2.44419	0.43331
$i = 1$	$-4.63685 \times 10^{-5}$	-1.34837	-0.68344
$i = 2$	$-5.36235 \times 10^{-4}$	1.76567	0.80121
$i = 3$	$2.70399 \times 10^{-4}$	—	-0.42937
$i = 4$	$-3.69906 \times 10^{-5}$	—	0.10581
$i = 5$	—	—	$-9.8755 \times 10^{-3}$

and the Mach number as

$$M = \frac{U_{Cp}}{\sqrt{\gamma R_a T_{Cp,in}}} \quad (32)$$

where the compressor blade tip speed is given as

$$U_{Cp} = \frac{\pi}{60} d_{Cp} N_{cr} \quad (33)$$

with the corrected rotational speed defined in terms of the rotational speed,  $N_{Cp}$ , as

$$N_{cr} = \frac{N_{Cp}}{\sqrt{\theta}} \quad (34)$$

The normalized temperature is defined as

$$\theta = \frac{T_{Cp,in}}{288} \quad (35)$$

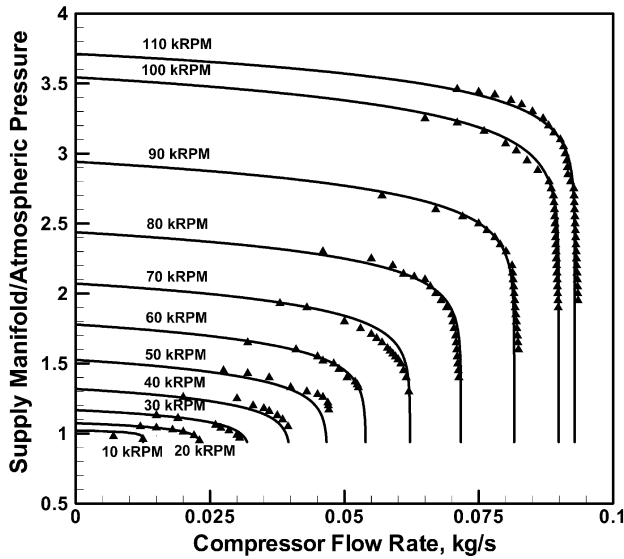


**Fig. 7** Compressor map for an Allied Signal compressor [9]. Experimental data are denoted using triangles, and the non-linear curve fitting [11] is denoted using solid lines

and the normalized pressure as

$$\delta = \frac{P_{Cp,in}}{P_{atm}} \quad (36)$$

The compressor map regression coefficients appearing in equations (28) to (30) for an Allied Signal compressor are given in Table 3 [12]. A comparison of the experimental (triangles) and the curve-fitted (solid lines) compressor maps is shown in Fig. 7.

## APPENDIX 2

### Water transport through the membrane

The flowrate of water through the membrane is controlled by two transport phenomena—electroosmotic drag of water molecules by the protons and back-diffusion from the cathode towards the anode—and is defined as [12]

$$W_{v,m} = M_v A_{fc} n \left( n_d \frac{i}{F} - D_w \frac{(c_{v,Ca} - c_{v,An})}{t_m} \right) \quad (37)$$

where the electroosmotic drag coefficient is given as

$$n_d = 0.0029 \mu_m^2 + 0.05 \mu_m - 3.4 \times 10^{-19} \quad (38)$$

with  $\mu_m$  being the mean water content in the membrane. The water content is defined as

$$\mu_i = \begin{cases} 0.043 + 17.81 a_i - 39.85 a_i^2 + 36.0 a_i^3, & 0 < a_i \leq 1 \\ 14 + 1.4(a_i - 1), & 1 < a_i \leq 3 \end{cases} \quad (i = m, An, Ca) \quad (39)$$

where the water vapour activity is defined as

$$a_i = \frac{x_{v,i} P_i}{p_{sat,i}} = \frac{P_{v,i}}{p_{sat,i}} \quad (i = An, Ca) \quad (40)$$

The average water vapour activity in the membrane is defined as

$$a_m = \frac{a_{An} + a_{Ca}}{2} \quad (41)$$

and the water diffusion coefficient is given as

$$D_w = D_\lambda \exp \left[ 2416 \left( \frac{1}{303} - \frac{1}{T_{fc}} \right) \right] \times 10^{-4} \quad (42)$$

with the preexponential term

$$D_\lambda = \begin{cases} 10^{-6}, & \mu_m < 2 \\ 10^{-6}[1 + 2(\mu_m - 2)], & 2 \leq \mu_m \leq 3 \\ 10^{-6}[3 - 1.67(\mu_m - 3)], & 3 < \mu_m < 4.5 \\ 1.25 \times 10^{-6}, & \mu_m \geq 4.5 \end{cases} \quad (43)$$

The water concentration

$$c_{v,i} = \frac{\rho_{m,dry}}{M_{m,dry}} \mu_i \quad (i = \text{An, Ca}) \quad (44)$$

### APPENDIX 3

#### Non-linear nozzle flowrate

The non-linear nozzle flowrate equation depends on the flow regime [13]

$$W = \begin{cases} \frac{C_D A_T p_u}{\sqrt{RT_u}} (\text{PR})^{1/\gamma} \left\{ \frac{2\gamma}{\gamma-1} [1 - (\text{PR})^{(\gamma-1)/\gamma}] \right\}^{1/2}, & \text{PR} = \frac{p_d}{p_u} > \text{PR}_{\text{crit}} \quad (\text{normal flow}) \\ \frac{C_D A_T p_u}{\sqrt{RT_u}} \gamma^{1/2} \left( \frac{2}{\gamma+1} \right)^{(\gamma+1)/2(\gamma-1)}, & \text{PR} = \frac{p_d}{p_u} \leq \text{PR}_{\text{crit}} \quad (\text{choked flow}) \end{cases} \quad (45)$$

where the critical pressure drop is defined as

$$\text{PR}_{\text{crit}} = \left( \frac{p_d}{p_u} \right)_{\text{crit}} = \left( \frac{2}{\gamma+1} \right)^{\gamma/(\gamma-1)} \quad (46)$$

and the subscripts  $u$  and  $d$  are used to denote upstream and downstream quantities respectively. When the pressure difference across the nozzle is small, the nozzle flowrate equation can be linearized, as given in equation (10).

### APPENDIX 4

#### Fuel cell stack voltage

The voltage of a fuel cell stack consisting of  $n$  fuel cells is given as [12]

$$v_{\text{st}} = n v_{\text{fc}} \quad (47)$$

where the voltage of a single fuel cell is defined as

$$v_{\text{fc}} = E - v_{\text{act}} - v_{\text{ohm}} - v_{\text{conc}} \quad (48)$$

with  $E$  being the open circuit voltage and  $v_{\text{act}}$ ,  $v_{\text{ohm}}$  and  $v_{\text{conc}}$  being the activation, ohmic and concentration

overpotentials respectively. By fitting experimental data to the phenomenological model equations, the open circuit voltage and the three overpotentials are respectively defined in reference [12] as

$$E = 1.229 - 0.85 \times 10^{-3}(T_{\text{fc}} - T_{\text{amb}}) + 4.3085 \times 10^{-5} T_{\text{fc}} \times \left[ \ln(1.01325 p_{\text{H}_2}) + \frac{1}{2} \ln(1.01325 p_{\text{O}_2}) \right] \quad (49)$$

$$v_{\text{act}} = v_0 + v_a (1 - e^{-c_1 i}) \quad (50)$$

with

$$v_0 = 0.279 - 8.5 \times 10^{-4}(T_{\text{fc}} - T_{\text{amb}}) + 4.308 \times 10^{-5} T_{\text{fc}} \left[ \ln \left( \frac{p_{\text{Ca}} - p_{\text{sat}}(T_{\text{fc}})}{1.01325} \right) + \frac{1}{2} \ln \left( \frac{0.1173(p_{\text{Ca}} - p_{\text{sat}}(T_{\text{fc}}))}{1.01325} \right) \right] \quad (51)$$

$$v_a = (-1.618 \times 10^{-5} T_{\text{fc}} + 1.618 \times 10^{-2}) \times \left( \frac{p_{\text{O}_2}}{0.1173} + p_{\text{sat}}(T_{\text{fc}}) \right)^2 + (1.8 \times 10^{-4} T_{\text{fc}} - 0.166) \left( \frac{p_{\text{O}_2}}{0.1173} + p_{\text{sat}}(T_{\text{fc}}) \right) + (-5.8 \times 10^{-4} T_{\text{fc}} + 0.5736) \quad (52)$$

$$c_1 = 10 \quad (53)$$

$$v_{\text{ohm}} = i R_{\text{ohm}} \quad (54)$$

with the fuel cell electrical resistance

$$R_{\text{ohm}} = \frac{t_m}{\sigma_m} \quad (55)$$

the membrane conductivity

$$\sigma_m = (b_{11} \mu_m - b_{12}) \exp \left[ b_2 \left( \frac{1}{303} - \frac{1}{T_{\text{fc}}} \right) \right] \quad (56)$$

$$b_{11} = 5.139 \times 10^{-3}, \quad b_{12} = 3.26 \times 10^{-3}, \quad b_2 = 350 \quad (57)$$

and

$$v_{\text{conc}} = i \left( c_2 \frac{i}{i_{\text{max}}} \right)^{c_3} \quad (58)$$

with

$$c_2 = \begin{cases} (7.16 \times 10^{-4} T_{fc} - 0.622) \left( \frac{p_{O_2}}{0.1173} + p_{sat}(T_{fc}) \right) \\ \quad + (-1.45 \times 10^{-3} T_{fc} + 1.68) \\ \quad \text{for } \left( \frac{p_{O_2}}{0.1173} + p_{sat}(T_{fc}) \right) < 2 \text{ atm} \\ (8.66 \times 10^{-5} T_{fc} - 0.068) \left( \frac{p_{O_2}}{0.1173} + p_{sat}(T_{fc}) \right) \\ \quad + (-1.6 \times 10^{-4} T_{fc} + 0.54) \\ \quad \text{for } \left( \frac{p_{O_2}}{0.1173} + p_{sat}(T_{fc}) \right) \geq 2 \text{ atm} \end{cases} \quad (59)$$

$$i_{max} = 2.2, \quad c_3 = 2 \quad (60)$$

It should be noted that all pressure quantities in this appendix are expressed in bars and  $p_{O_2}$  refers to the outlet partial pressure of oxygen in the cathode.

PEM fuel cell polarization curves at different pressures of the fully humidified air in the cathode and at  $T_{st} = 353$  K are shown in Fig. 8. The effect of air humidity on the PEM fuel cell polarization curve at  $T_{st} = 353$  K and  $p_{Ca} = 1.0 \times 10^5$  Pa and  $p_{Ca} = 4.0 \times 10^5$  Pa is shown (as dashed curves) in Fig. 8. It should also be noted that the approximation that the stack temperature remains constant under the various operating conditions studied in the present

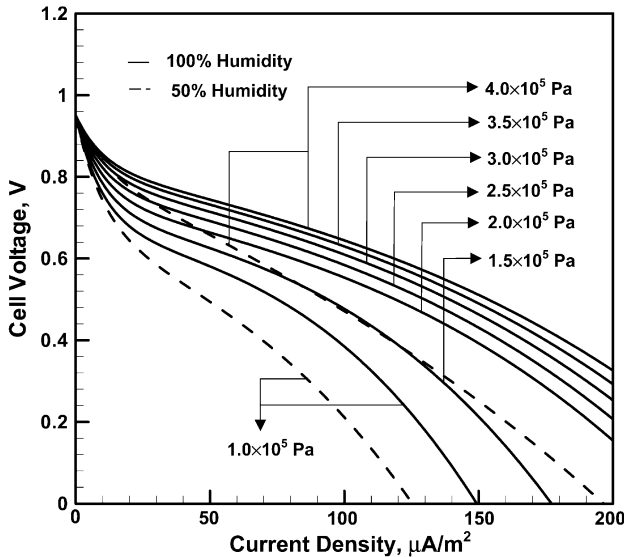


**Fig. 8** Polarization curves for a single PEM fuel cell at 353 K and at different pressures of the fully humidified (solid lines) and 50 per cent relative humidified (dashed lines) air in the cathode

work entails strict temperature control, since the airflow can have a significant effect on the rate of heat generation.

**APPENDIX 5**

**Linearized system matrices**

The system matrices obtained by linearizing the non-linear model of the PEM fuel cell around a nominal point corresponding to  $P_{net}^{max} = 39.825$  kW,  $I_{st} = 190$  A,  $v_{CM}^{opt} = 187.5$  V and  $\lambda_{O_2}^{opt} = 2.33$  are given below

$$A = \begin{bmatrix} -6.5421 & 0 & -10.8897 & 0 \\ 0 & -161.099 & 0 & 0 \\ -18.68 & 0 & -46.8923 & 0 \\ 0 & 0 & 0 & -13.07139 \\ 1.2956 & 0 & 2.96019 & 0.368135 \\ 16.641 & 0 & 38.0211 & 4.728388 \\ 0 & -393.984 & 0 & 0 \\ 2.022 & 0 & 4.61989 & 0 \\ 83.82553 & 0 & 0 & 24.52081 \\ 49.44071 & 0 & -18.12282 & 0 \\ 275.9257 & 0 & 0 & 161.4285 \\ 198.4325 & 0 & 0 & 0 \\ -39.9678 & 0.104351 & 0 & 0 \\ -488.877 & 0 & 0 & 0 \\ 117.8518 & 0 & -99.63699 & 0 \\ 0 & 0 & 0 & -51.3409 \end{bmatrix}$$

$$B_u = \begin{bmatrix} 0 \\ 0 \\ 0 \\ 2.7569 \\ 0 \\ 0 \\ 0 \\ 0 \\ 0 \\ 0 \end{bmatrix}, \quad B_w = \begin{bmatrix} -0.03159 \\ -0.00395 \\ 0 \\ 0 \\ 0 \\ 0 \\ -0.09025 \\ 0 \end{bmatrix}$$

$$D_{zu} = \begin{bmatrix} -0.1158 \\ 0 \end{bmatrix}, \quad D_{zw} = \begin{bmatrix} 0.167856 \\ -0.01042 \end{bmatrix}$$

$$C_z = \begin{bmatrix} 2.66013 & 2.03688 & -0.10896 & 0.1244 \\ -0.6375 & 0 & -1.45555 & 0 \\ & & 0 & 0 \\ & & 0 & 0 \\ & & 13.8927 & 0 \end{bmatrix}$$



# Journal of Power and Energy

Proceedings of the Institution of Mechanical Engineers Part A

## OFFPRINTS/JOURNAL ORDER FORM

To ensure that you receive the offprints *or* Journal you require please return this form with your corrections.

Manuscript Number: **A/2003/000067**

Number of pages: 13

Authors: Mica Grujicic, K M Chittajallu, E H Law and J T Pukrushpan

If you would prefer to receive a free copy of the Journal issue *instead of* 25 free offprints please indicate below:

Quantity	1 copy of the Journal issue	25 offprints	100 offprints	250 offprints	500 offprints
Cost	free	free	£65	£124	£215

**Please supply ..... offprints / 1 copy of the Journal issue\* and forward to the following address:**

**\*Delete as appropriate**

Professor Mica Grujicic  
Clemson University  
Department of Mechanical Engineering  
241 Fluor Daniel Bldg.  
Clemson  
SC  
29634-0921  
USA

The above prices do not include postage and packaging. These charges apply only to bona fide authors who need offprints for their own private use. Offprints required for any other purpose (e.g. publicity, promotion) are subject to a different scale of charges which will be quoted on request.

Any orders received after the return of proofs will be treated as reprints, which will be charged at a higher rate. Quotations for reprints will be provided on request.